Published in final edited form as:

J Magn Reson. 2016 December ; 273: 124–129. doi:10.1016/j.jmr.2016.10.014.

Diffusion-mediated ^{129}Xe Gas Depolarization in Magnetic Field Gradients During Continuous-flow Optical Pumping

Alex Burant[1,2] and **Rosa Tamara Branca**[1,2,*]

[1]Department of Physics and Astronomy, University of North Carolina at Chapel Hill, US

[2]Biomedical Research Imaging Center, University of North Carolina at Chapel Hill, US

Abstract

The production of large volumes of highly polarized noble gases like helium and xenon is vital to applications of magnetic resonance imaging and spectroscopy with hyperpolarized (HP) gas in humans. In the past ten years, ^{129}Xe has become the gas of choice due to its lower cost, higher availability, relatively high tissue solubility, and wide range of chemical shift values. Though near unity levels of xenon polarization have been achieved in-cell using stopped-flow Spin Exchange Optical Pumping (SEOP), these levels are currently unmatched by continuous-flow SEOP methods. Among the various mechanisms that cause xenon relaxation, such as persistent and transient xenon dimers, wall collisions, and interactions with oxygen, relaxation due to diffusion in magnetic field gradients, caused by rapidly changing magnetic field strength and direction, is often ignored. However, during continuous-flow SEOP production, magnetic field gradients may not have a negligible contribution, especially considering that this methodology requires the combined use of magnets with very different characteristics (low field for spin exchange optical pumping and high field for the reduction of xenon depolarization in the solid state during the freeze out phase) that, when placed together, inevitably create magnetic field gradients along the gas-flow-path. Here, a combination of finite element analysis and Monte Carlo simulations is used to determine the effect of such magnetic field gradients on xenon gas polarization with applications to a specific, continuous-flow hyperpolarization system.

Graphical Abstract

[*]Correspondence to: Rosa Tamara Branca, Ph.D. Department of Physics and Astronomy, University of North Carolina at Chapel Hill, Chapel Hill, NC 27599, USA. rtbranca@unc.edu.

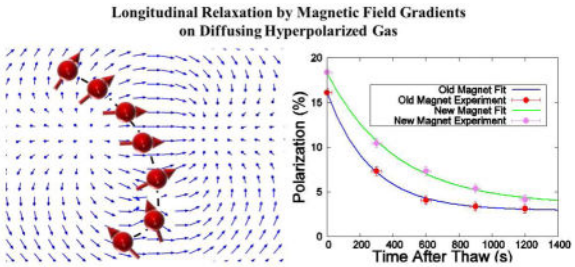

Keywords

Gas-phase relaxation; Hyperpolarized ^{129}Xe; Longitudinal relaxation; Magnetic field gradients; Continuous-flow; Magnetic resonance imaging

I. Introduction

In the past fifteen years, the number of viable applications of hyperpolarized gas for magnetic resonance imaging and spectroscopy has drastically increased [1]. The initial isotope of choice for gas hyperpolarization by Spin Exchange Optical Pumping (SEOP) was ^{3}He, and now large volumes of highly polarized ^{3}He are achievable [2,3]. However, due to increasing demand for ^{3}He in many applications and an extremely limited supply source (tritium decay from both nuclear fusion warheads and tritium produced using commercial nuclear reactors), a ^{3}He supply crisis has begun [4]. An effective alternative to ^{3}He was found in ^{129}Xe, which can now reach similar polarization levels for comparable volumes of gas [5]. Thanks to its high tissue solubility, xenon gas—originally used solely for lung ventilation studies—is now being used for a variety of imaging and spectroscopic applications, including molecular imaging with biosensors, detection of brown adipose tissue in mammals, high-resolution spectroscopy and chemical shift imaging in the human brain, among many others [6–10]. For each of these applications, the production of large volumes of highly polarized gas is essential.

Originally, noble gas was polarized by spin exchange optical pumping using a batch method. Specifically, the unpolarized noble gas is flowed into an optical pumping cell containing an alkali metal. The alkali metal is heated until an optically thick vapor is created and then it is illuminated by laser light to induce optical pumping. Spin exchange follows via collisions between alkali metal atoms and the noble gas atoms present in the cell. Once the gas reaches the desired, achievable polarization, the cell is cooled to allow the alkali metal to freeze out and the polarized gas is transferred to a storage container. The batch method is the only method used to polarize helium via spin exchange optical pumping due in part to the low spin exchange rates between helium and rubidium, which cause pump up times on the order of hours. The batch method has also been used for polarizing xenon [11]. However, the maximum achievable polarization for xenon occurs at low xenon partial pressures, meaning clinically relevant volumes (~1 L) of highly polarized (>25%) xenon can be more difficult to achieve using the batch method [12].

Fortunately, the spin exchange rates between xenon and rubidium are three orders of magnitude higher than between helium and rubidium, decreasing the pump-up time from hours to minutes and allowing xenon to be polarized via continuous-flow spin exchange optical pumping [13,14]. In this method, a mixture of xenon, nitrogen, and helium are continuously flowed through an optical cell that is illuminated by laser light. Typically, a lean mixture of xenon (between 1–5%) is used to limit the spin destruction mechanism due to spin-non-conserving, binary, Rb-Xe collisions [15]. Helium is added as a buffer gas to pressure-broaden the rubidium absorption line and nitrogen is added to quench the fluorescence of excited rubidium [16,17]. The xenon gas atoms become polarized by spin exchange with an optically thick alkali metal vapor within the cell, in the same way as the batch method, but continue to flow out of the cell where they are separated from the mixture and collected using a liquid nitrogen cold trap. Once the desired volume of xenon is frozen in the cold trap, the flow of gas is stopped, the optical cell is closed, and the polarized xenon is thawed and transferred to a storage container. Continuous-flow xenon hyperpolarization is the most widely used method for clinical applications as it offers the potential to produce large volumes of gas in a shorter amount of time than the batch method. Unfortunately, the current achievable polarizations are lower than those of the batch method due to a number of confounding factors.

One possible source of spin relaxation is diffusion through magnetic field gradients. Gradient-induced spin relaxation has been shown to be a significant source of relaxation in the fringe field of superconducting magnets but is often ignored for hyperpolarized xenon in both batch method and continuous-flow polarizers [18]. While most batch method systems contain one or more sets of Helmholtz coils to generate a low (tens of gauss), uniform magnetic field necessary for SEOP, continuous-flow polarization systems contain an additional magnet used to generate a much higher magnetic field (kilogauss) in which the gas is stored in the frozen state during the collection process. Depending on the relative configuration of these two magnets, the probability that the polarized gas, traveling from the optical cell contained within the low field to the cold trap contained within the high field, flows through a region where the magnetic field rapidly changes direction is particularly high. In this paper, by using both computer simulations and experimental measurements of longitudinal relaxation time, we look at the effect of ^{129}Xe diffusion through the magnetic field gradients that are present in a commercial, continuous-flow polarizer equipped with a single pair of Helmholtz coils and two different, interchangeable, permanent magnets. We show that, in some cases, diffusion through magnetic field gradients has a non-negligible effect on the final polarization level of the gas.

II. Materials and Methods

A. Theory

Longitudinal relaxation, also known as T_1 relaxation, involves the interaction of nuclear spins with the surrounding environment and, through energy exchange, causes the relaxation of a nuclear spin system back to thermal equilibrium. The contribution of magnetic field inhomogeneities to the longitudinal relaxation of hyperpolarized gases has been extensively studied and is well described by the following relation [19,20]:

$$\frac{1}{T_1} = D\frac{|\nabla B_T|^2}{{B_0}^2}\left(1+{\Omega_0}^2{\tau_c}^2\right)^{-1} \quad (1)$$

where D represents the diffusion coefficient for the hyperpolarized gas, B_0 is the magnitude of the mean magnetic field, and ∇B_T is the transverse component of the spatial gradient of B_0. The extra factor, $(1+\Omega_0{}^2\tau_c{}^2)^{-1}$ accounts for rotation of spins between kinetic collisions, where Ω_0 is the Larmor frequency and τ_c, the diffusion correlation time, is the time between collisions. Since this factor is nearly unity for a mean magnetic field below 20 T and under the experimental conditions of interest presented here, it will be omitted.

Most often, the mean magnetic field, B_0, is assumed to point along a well-defined quantization axis and the spatial gradient of the mean magnetic field is assumed to be independent of position [21]. Though these assumptions may be valid within the optical pumping cell, which is contained within the low, polarizing field generated by a Helmholtz coil, they are not valid when the gas flows from a region in which the field is on the order of a few tens of gauss to a region where the field is on the order of thousands of gauss. For the work presented here, these assumptions are removed and the local magnetic field is used along with the transverse component of the spatially-dependent gradient of B_0. In using the local magnetic field strength rather than the mean magnetic field along a well-defined quantization axis, it is important to note that a large relaxation rate in Eq. (1) can be obtained whenever the magnetic field rapidly changes direction and assumes very low values, like in the case of a zero-field crossing.

B. Simulation

Simulations were first performed to determine the distribution of the magnetic field throughout the region in which xenon freely diffuses during the polarization process in a Polarean 9800 ^{129}Xe Hyperpolarizer system (Polarean Inc., Durham, NC, USA), a system currently used by several research groups around the world. In this system, a single pair of Helmholtz coils creates the polarization field, while the holding field is created by a permanent magnet. Simulations were performed for two different permanent magnet designs, both of which are currently available in our lab: one originally provided with the Polarean 9800 ^{129}Xe Hyperpolarizer system and one currently provided with the Polarean 3777 upgrade module. Full-scale models of the two setups, which were identical except for the design of the permanent magnet, were developed using the computer-aided design (CAD) software SolidWorks (Dassault Systèmes SolidWorks Corp., Vèlizy-Villacoubly, France) and can be seen in Fig. 1. Figure 2 shows a three-dimensional view of both permanent magnet designs. Of note for the old magnet design are the steel top containing two holes and an open front while the new magnet design has the steel top removed and a closed front.

The CAD models were then imported into the finite element analysis software COMSOL Multiphysics (COMSOL, Stockholm, Sweden) where finite element analysis was used to calculate the distribution of the magnetic flux density. The Helmholtz coil consisted of two 40.3 cm ID coils spaced 23.98 cm apart that were made of 200 turns of 14 AWG copper

wire. A current of 2.99 A was used in each coil to create a field within the homogeneous region of approximately 20 G. The remnant flux density for each permanent magnet was adjusted within the simulation until a center point magnetic field of 2000 G was achieved. These field strengths were chosen to match, within 5%, the field distribution experimentally measured on our polarizer system using a gauss meter.

Data from the COMSOL simulations was used to calculate a theoretical T_1 value using a custom MATLAB (MathWorks, Natick, MA, USA) script. Specifically, Monte Carlo simulations of gas diffusion through the computed magnetic field gradient were used to determine the depolarization of xenon nuclear spins as the atoms freely diffused throughout the region highlighted in red in Fig. 1 after the solid xenon had been thawed. For these simulations, a diffusion coefficient of pure xenon of 0.0132 cm^2/s was determined by the Fuller-Schettler-Giddings equation for a temperature of 293.15 K and a pressure of 63 psi [22]. For each time step, the relaxation rate was calculated using Eq. (1). A time-averaged T_1 value was first calculated for each spin and then a final average T_1 value was calculated for an entire ensemble of 100 spins.

C. Experiment

Experiments were performed on the Polarean 9800 ^{129}Xe Polarizer system. Measurements were made for each permanent magnet design. A schematic of the experimental setup and gas-flow-path within the polarizer system is shown in Fig. 1, with the volume where the gas freely diffuses after thawing highlighted in red. The gas, consisting of a mixture of 1% xenon at natural abundance (26.4% ^{129}Xe), 10% nitrogen, and 89% helium (Global Specialty Gases, Bethlehem, PA, USA), is pre-saturated with rubidium vapor within a pre-saturation column that is maintained at 438 K and located right before the cell inlet (not shown in figure 1). The rubidium-saturated gas is then flowed at a rate of 1.5 SLM and at a total pressure of 60 psi into the optical pumping cell, which resides inside a single pair of Helmholtz coils and in which the temperature is maintained at 358 K. The optical cell is illuminated by a 60 W diode laser with a center wavelength of 794.6 nm and FWHM of 0.2 nm (Spectra-Physics, Santa Clara, CA, USA). An on-board NMR system, located on the surface of the optical pumping cell, is used to monitor the ^{129}Xe gas polarization within the optical pumping cell. From the optical cell, the gas flows to the cold finger, located within the permanent magnet region, where the gas is condensed and stored for a total “collection” time of eleven minutes, yielding a total xenon gas volume of 165 ml. At the end of the collection time, the gas is quickly thawed and free to diffuse within the region highlighted in red in Fig. 1.

To measure the relaxation induced by the magnetic field gradients generated by the two permanent magnet designs, several batches of hyperpolarized gas were produced as described above to allow the gas to diffuse within the region highlighted in red in Fig. 1 for different amounts of time after the freeze/thaw cycle. After this time, the gas was dispensed into a Tedlar bag, which was quickly (1–2 s) placed on a calibrated Polarean 2881 Polarization Measurement Station (Polarean Inc., Durham, NC, USA), to measure the gas polarization level. Gas polarization level as a function of the free diffusion time was then fit

to a mono-exponential decay curve in Mathematica (Wolfram Research Inc., Champaign, IL, USA) to derive the mean T_1 relaxation time for both permanent magnet designs.

III. Results

Field maps for both permanent magnet designs are shown in Figure 5. COMSOL simulations showed that the old permanent magnet generates an arc-shaped region in which the field rapidly changes direction and assumes values as low as 0.0138 G. This region was located in one of the top holes through which the gas was entering and exiting the cold finger, affecting primarily the gas flowing out of the cold finger (Fig. 4). Based on the field distribution simulations, it was anticipated that the old magnet was going to lead to faster xenon relaxation than the new magnet. The MATLAB simulations supported this prediction, with the old permanent magnet design generating a field distribution that relaxed the spins with an average T_1 of 591±70 s and the new permanent magnet producing a field distribution that relaxed the spins with an average T_1 of 1644±90 s.

When the T_1 was measured experimentally, a T_1 value of 268±14 s was measured for the original magnet, while a T_1 value of 417±40 s was measured for the new magnet design. The experimental data and fit can be seen in Fig. 6. As expected, these relaxation values were lower than those found using the simulations, as they contain a contribution from wall collisions and binary collisions between xenon atoms that were ignored in the simulations. Since the relaxation rates due to wall collisions and binary collisions are expected to be identical for the two different magnet designs, their values can be estimated by using the experimental relaxation value and the computed relaxation value due to magnetic field inhomogeneities in the following fashion:

$$\left(\frac{1}{T_1}\right)_{Exp} = \left(\frac{1}{T_1}\right)_{MFI} + \left(\frac{1}{T_1}\right)_{CR} \quad (2)$$

where *Exp* indicates the experimentally determined T_1 value, *MFI* indicates the relaxation contribution due to magnetic field inhomogeneities, and *CR* is the collisional relaxation contribution consisting of wall relaxation and transient and persistent xenon dimers.

By using this relation, the estimate for the combined contribution of wall collisions and binary collisions to the longitudinal relaxation time was on the order of 500 s for both magnet designs (488±70 s for the original magnet design and 558±70 s for the new magnet design). In pure xenon, Xe-Xe molecular relaxation is known to be the dominant fundamental relaxation mechanism below 14 amagat, giving a relaxation time on the order of hours [23]. The experiments performed in this paper were within this regime at a calculated xenon density of 4 amagat. As such, it is reasonable to assume that the major contribution to gas-phase relaxation, at least in this system, is likely to be wall collisions with perfluroalkoxy (PFA), which makes up most of the tubing that connects the cold finger to the gas outlet, and uncoated Pyrex, which makes up the cold finger. Wall relaxation times for uncoated Pyrex have been measured at temperatures of ~80°C to range from 200 s to as

high as 1300 s in exceptional cases [24]. Therefore, the number obtained here for the T_1 due to wall relaxation is not in disagreement with the range of values previously measured.

The experimental and simulation results shown here indicate that the crossing of regions in which the magnetic field rapidly changes direction and assumes negligible values can be a major relaxation mechanism and care should be taken to avoid creating such gradients within the hyperpolarized gas-flow-path. To this end, the flux return on the new magnet design represents a significant improvement over the previous design, eliminating such gradients and thus better preserving the nuclear spin polarization.

IV. Conclusions

The influence of strong magnetic field gradients on the relaxation of hyperpolarized xenon during continuous-flow SEOP was studied using a combination of finite element method analysis and Monte Carlo simulations. Simulation results were then compared to experimental T_1 values obtained from a commercially available polarizer system using two different permanent magnet designs, which were able to generate significantly different magnetic field distributions within the gas-flow-path. Specifically, one of the magnets produced a region in which the magnetic field rapidly changed direction, causing a faster relaxation of xenon atoms diffusing from the cold finger to the collection bag. The relative configuration and the geometry of the magnets used for continuous-flow SEOP requires careful design in order to avoid the generation of regions in which the magnetic field rapidly changes direction where the gas is able to diffuse and relax. While magnetic field gradients should not be ignored during continuous-flow SEOP, this work suggests that, in the absence of such strong gradients, wall collisions are the major contributing factor to gas-phase spin relaxation.

Acknowledgments

This work was supported by Dr. Branca’s startup grant from the Department of Physics and Astronomy and Lineberger Cancer Center at the University of North Carolina at Chapel Hill and by the NIH grant number R01DK108231.

References

1. Lilburn DML, Pavlovskaya GE, Meersmann T. J Magn Reson. 2013; 229:173. [PubMed: 23290627]
2. Bouchiat MA, Carver TR, Varnum CM. Phys Rev Lett. 1960; 5:373.
3. van Beek EJR, Wild JM, Kauczor HU, Schreiber W, Mugler JP III, de Lange EE. J Magn Reson Imaging. 2004; 20:540. [PubMed: 15390146]
4. Cho A. Science. 2009; 326:778. [PubMed: 19892947]
5. Nikolaou P, Coffey AM, Walkup LL, Gust BM, Whiting N, Newton H, Barcus S, Muradyan I, Dabaghyan M, Moroz GD, Rosen MS, Patz S, Barlow MJ, Chekmenev EY, Goodson BM. Proc Natl Acad Sci USA. 2013; 110:14150. [PubMed: 23946420]
6. Shapiro MG, Ramirez RM, Sperling LJ, Sun G, Sun J, Pines A, Schaffer DV, Bajaj VS. Nature Chem. 2014; 6:629. [PubMed: 24950334]
7. Branca RT, He T, Zhang L, Floyd CS, Freeman M, White C, Burant A. Proc Natl Acad Sci USA. 2014; 111:18001. [PubMed: 25453088]
8. Rao M, Stewart NJ, Norquay G, Griffiths PD, Wild JM. Magn Reson Med. 2016; 75:2227. [PubMed: 27080441]

9. Kaiser LG, Meersmann T, Logan JW, Pines A. Proc Natl Acad Sci USA. 2000; 97:2414. [PubMed: 10706617]
10. Moule AJ, Spence MM, Han SI, Seeley JA, Pierce KL, Saxena S, Pines A. Proc Natl Acad Sci USA. 2003; 100:9122. [PubMed: 12876195]
11. Baranga AB, Appelt S, Romalis MV, Erickson CJ, Yound AR, Cates GD, Happer W. Phys Rev Lett. 1998; 80:2801.
12. Fink A, Baumer D, Brunner E. Phys Rev A. 2005; 72:053411.
13. Grover BC. Phys Rev Lett. 1978; 40:391.
14. Jau YY, Kuzma NN, Happer W. Phys Rev A. 2003; 67:022720.
15. Driehuys B, Cates GD, Miron E, Sauer K, Walter DK, Happer W. Appl Phys Lett. 1996; 69:1668.
16. Romalis MV, Miron E, Cates GD. Phys Rev A. 1997; 56:4569.
17. Wagshul ME, Chupp TE. Phys Rev A. 1994; 49:3854. [PubMed: 9910682]
18. Zheng W, Cleveland ZI, Möller HE, Driehuys B. J Magn Reson. 2011; 208:284. [PubMed: 21134771]
19. Gamblin RL, Carver TR. Phys Rev. 1965; 138:A946.
20. Schearer LD, Walters GD. Phys Rev. 1965; 139:A1398.
21. Cates GD, Schaefer SR, Happer W. Phys Rev A. 1988; 37:2877.
22. Fuller EN, Schettler PD, Giddings JC. Ind Eng Chem. 1966; 58:18.
23. Chann B, Nelson IA, Anderson LW, Driehuys B, Walker TG. Phys Rev Lett. 2002; 88:113201. [PubMed: 11909399]
24. Zeng X, Miron E, Van Wigngaarden WA, Schreiber D, Happer W. Phys Lett. 1983; 96A:191.

Highlights

- Relaxation of ^{129}Xe from magnetic field gradients not negligible in all instances.
- Simulations revealed zero-field crossing in one holding magnet design.
- Newly designed holding magnet significantly improves longitudinal relaxation.
- Largest contribution to relaxation of ^{129}Xe in cold finger is wall collisions.

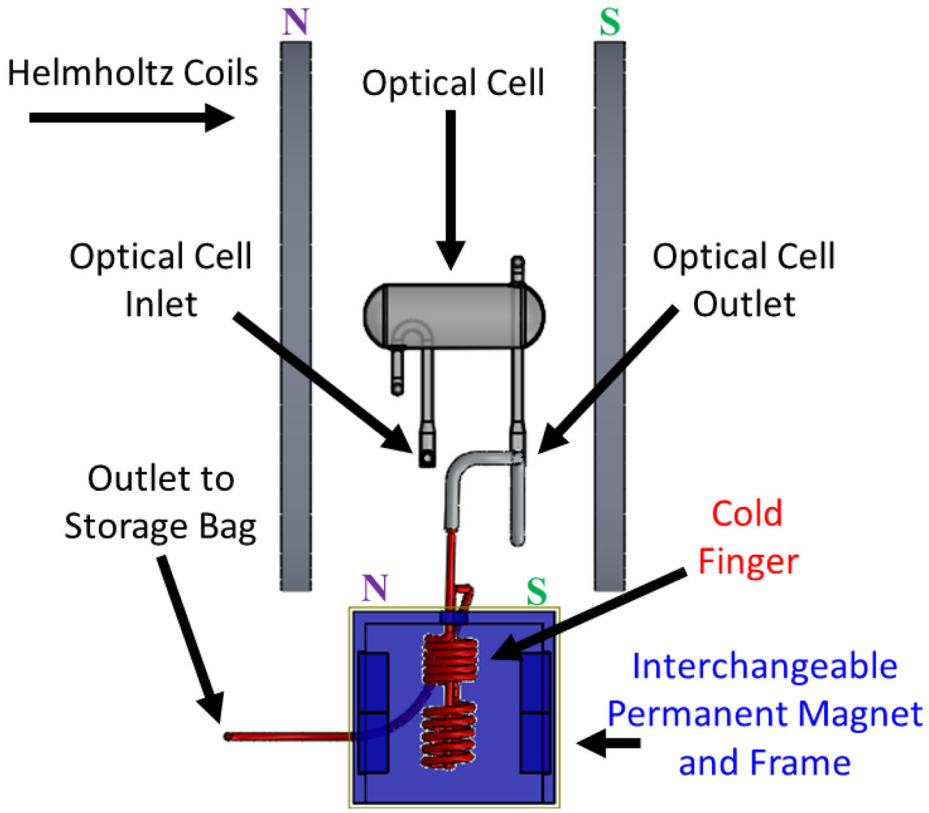

FIG. 1.

3D model of the continuous-flow polarization setup used in this work. The setup includes the Helmholtz coil, the optical cell, the cold finger, and the interchangeable permanent magnet and frame (highlighted in blue). The interchangeable permanent magnet allowed for an easy change to the distribution of the magnetic field in the region in which the gas diffuses after thawing, colored in red. North (N) and South (S) magnetic poles have been labeled to show the direction of the magnetic field.

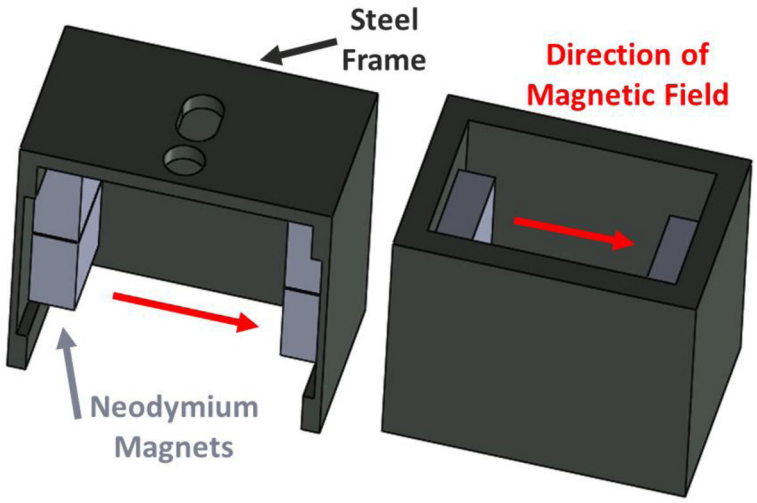

FIG. 2.

Three-dimensional view of the two different permanent magnets that were tested via simulation and experimentally. Left: Original magnet with closed top and open front showing the 4 rare-earth magnets (2 on each side). Right: New magnet with open top and closed front. In this case, the field is created by 2 rare-earth magnets (1 on each side). Direction of the magnetic field is shown for both magnet designs.

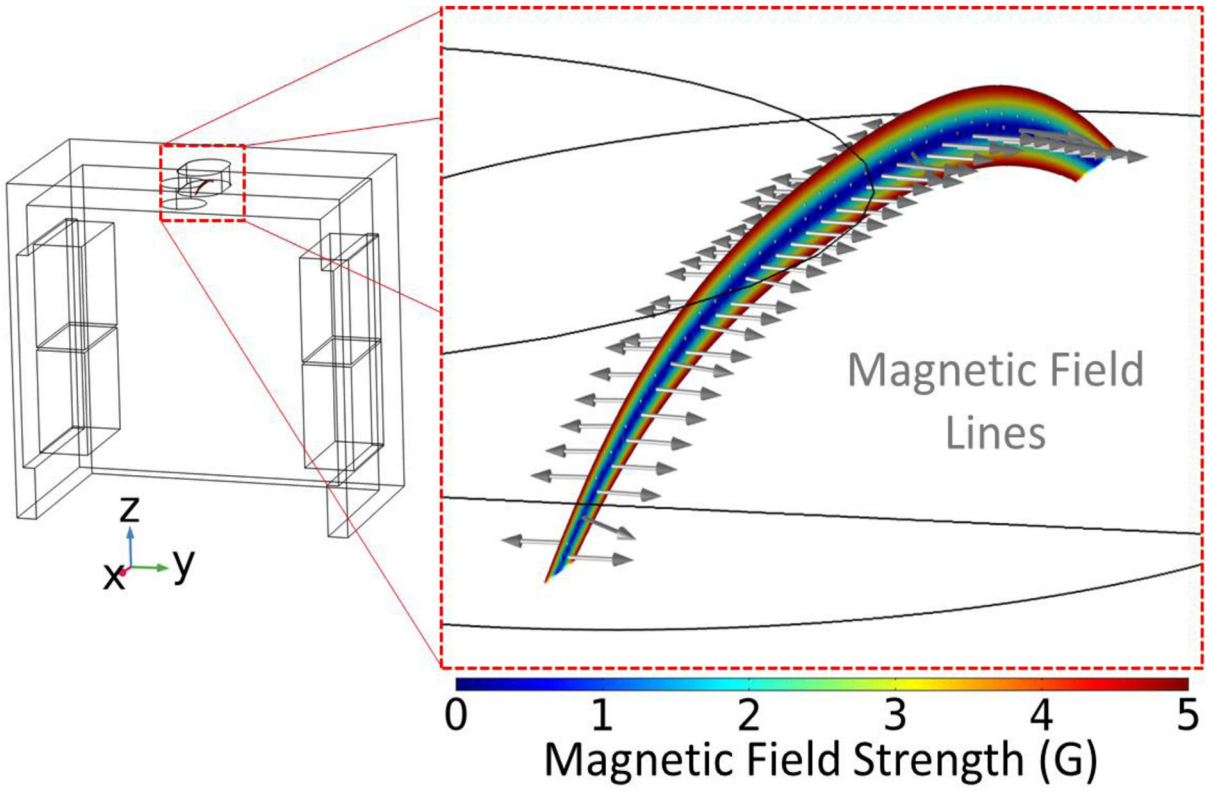

FIG. 3.

Surface plot showing the region, located within the hole at the top of the old permanent magnet, in which the magnetic field rapidly changes direction and, in some places, assumes a zero value. Left: Full view of the old magnet design with the location in which the magnetic field rapidly changes direction and assume negligible values highlighted. Right: Close up view of the same region. Color scale represents the magnetic field strength in gauss. Arrows represent the magnetic field lines. Note the successive arrows pointing in opposite directions indicating the presence of a zero magnetic field.

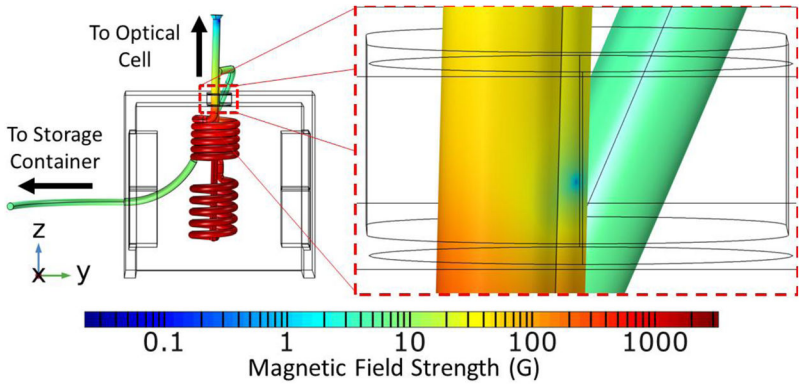

FIG. 4.

View of magnetic field strength for the old magnet design originally shipped with the polarizer. The close up view shows the area of the cold finger outlet affected by the region in which the field rapidly changes direction. A logarithmic color scale is used to highlight the areas in which the field assumes negligible values.

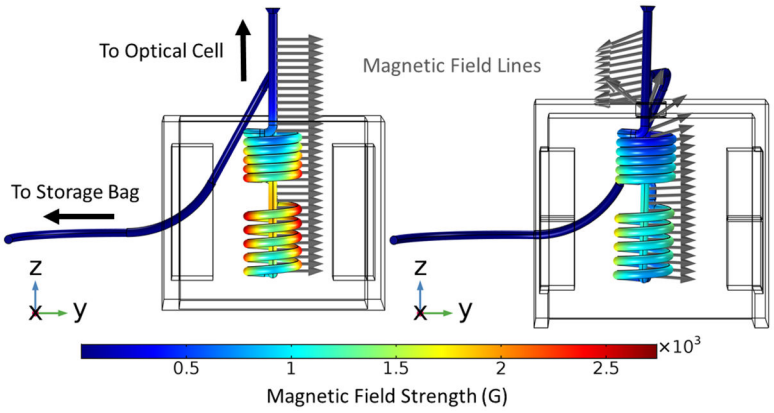

FIG. 5.

Strength of the magnetic field within the volume accessible, after thawing, to the polarized gas, before it is dispensed in a plastic bag. Left: magnetic field strength and direction as generated by the new magnet design. Right: magnetic field strength and direction as generated by the original magnet design. Note the drastic change in the magnetic field orientation present on the top of the original magnet design near the cold finger (spiral vessel) outlet, a region in which the gas is allowed to diffuse after thawing.

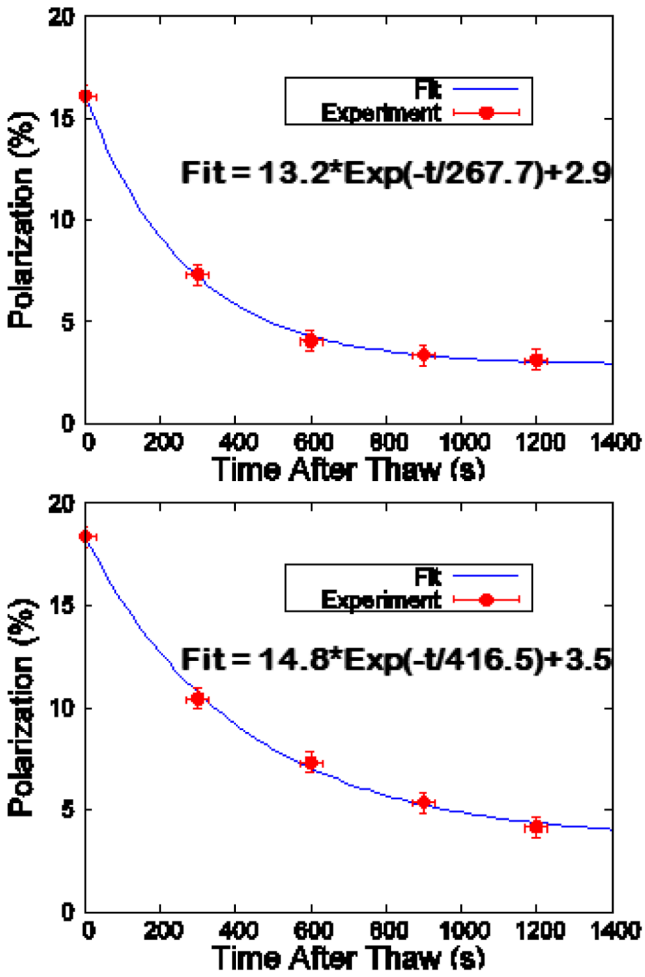

FIG. 6.

T_1 relaxation curves of hyperpolarized xenon gas due to magnetic field gradients generated by the two permanent magnets. For each permanent magnet, five separate batches of polarized gas were produced. The gas was then allowed to freely diffuse for varying amounts of time in the accessible volume highlighted in red in Figure 1. Top: relaxation curve for the old magnet with maximum polarization of 16.1% and T_1 of 268 s. Bottom: relaxation curve for the new magnet with maximum polarization of 18.4% and T_1 of 417 s.